On the use of EMI for the assessment of dental implant stability

Emma La Malfa Ribolla[a], Piervincenzo Rizzo[a,*], Vincenzo Gulizzi[b]
[a] Laboratory for NDE and SHM Studies, Department of Civil and Environmental Engineering, University of Pittsburgh, Pittsburgh, PA, USA 15261; [b] Department of Civil, Environmental and Materials Engineering, University of Palermo, Palermo, Italy 90128

ABSTRACT

The achievement and the maintenance of dental implant stability are prerequisites for the long-term success of the osseointegration process. Since implant stability occurs at different stages, it is clinically required to monitor an implant over time, i.e. between the surgery and the placement of the artificial tooth. In this framework, non-invasive tests able to assess the degree of osseointegration are necessary. In this paper, the electromechanical impedance (EMI) method is proposed to monitor the stability of dental implants. A 3D finite element model of a piezoceramic transducer (PZT) bonded to a dental implant placed into the bone was created, considering the presence of a bone-implant interface subjected to Young's modulus change. The numerical model was validated experimentally by testing bovine bone samples. The EMI response of a PZT, bonded to the abutment screwed to implants inserted to the bone, was measured. To simulate the osseointegration process a pulp canal sealer was used to secure the implant to the bone. It was found that the PZT's admittance is sensitive to the stiffness variation of the bone-implant interface. The results show that EMI-based method is able (i) to evaluate the material properties around the implant, and (ii) to promote a novel non-invasive monitoring of dental implant surgical procedure.

Keyword: Electromechanical impedance method, Dental Implants, Finite Element Method.

1. INTRODUCTION

In the past decades, dental implants have become an available treatment for completely and partially edentulous patients [1]. The most common clinically used implant therapy is based on the two-stages protocol advanced by Branemark [2]. The first step consists of the surgical insertion of the implant into the jawbone. At this stage, the primary implant stability is achieved as an outcome of the mechanical engagement with the bone [3]. The second step consists of screwing the abutment to the implant and connecting the crown (artificial tooth) to the abutment. Between the first and the second stage, a healing time that ranges from three to six months is strictly necessary to let the implant to be mechanically interlocked with the bone by means of a biological bone formation and remodeling (secondary stability). Since marginal bone change around implants can be related to multiple factors [4], such as implant design and chemical composition, topography of the implant surface, the status of the host bone bed and its intrinsic healing potential, the loading conditions applied, the implant therapy still faces many challenges in treatment outcomes. In addition, the extended healing time needs to be shortened in order to accommodate the growing patients' demands.

To make the therapy more cost-effective and to assess the degree of osseointegration during the healing time, several non-invasive methods have been proposed in the last few decades. These methods can be classified in two main categories, imaging and biomechanical techniques. Radiographic evaluation, computer tomography, magnetic resonance imaging, x-ray micro-computed tomography [5-6] belong to the first category. Such methods allow estimating the bone architecture before the surgery and observing changes in bone quality and quantity after the surgery. However, because imaging methods involve bulkiness and subject patients to radiations, biomechanical methods may offer advantages over the imaging ones. Probably the most common biomechanical systems are the Periotest® and the Osstell® which are commercially available [7-8]. The first one involves the use of a tappet accelerated by an electromagnet which impacts the tooth several times. The measure of stability is obtained by measuring the contact time between the tappet and the

*pir3@pitt.edu; phone 412-624-9575; fax 412-624-0135; http://www.pitt.edu/~pir3/

tooth, i.e. the lower the contact time, the more stable is the implant. The Osstell® system is based on the resonance frequency analysis (RFA) and involves the use of a L-shaped transducer screwed to the implant and excited by a sinusoidal signal. The indicator of stability is the resonance frequency of the implant, i.e. the higher the resonance frequency, the more stable is the implant. Despite commercially diffused, it has been proved that both Periotest® and Ossetell® cannot evaluate the peri-implant tissue conditions [9]. Moreover, their operation is influenced by factors such as bone density, upper or lower jaw, abutment length and supra-crestal implant length [10].

In the last few years, researchers at University of Pittsburgh have proposed the electromechanical impedance method (EMI) as a novel tool to assess the stability of dental implants [11-12]. This paper presents some fo the latest advancements. The method consists of bonding or embedding one or more piezoceramic transducers (PZTs) to the host element, to be monitored. If subjected to an electric field, the transducer induces low to high frequency structural excitations, which affect the transducer's electrical admitance. Since the transducer's electrical admittance is related to the mechanical impedance of the host structure, it can indirectly assess the health of the host element.

Even though EMI was widely used for the health monitoring of civil, aerospace and mechanical engineering infrastructures [13-14], its application in biomechanical field is rare [15]. In this research, we study both numerically and experimentally the osseointegration process, assumed as a healing process which affects the stiffness properties of the bone-implant interface. Numerically, the electromechanical coupling between the host structure and the bonded PZT is simulated by means of a 3D finite element model run in ANSYS. Experimentally, we used a commercial abutment and implant interlocked into *in vitro* bovine bone sample by means of a root canal sealer. The PZT admittance is measured by means of a small and inexpensive electrical circuit connected to a data acquisition system driven in LABVIEW.

2. ELECTROMECHANICAL IMPEDANCE METHOD

The mechanical impedance (Z) of a point on a structure is the ratio of the force applied at the point to the resulting velocity at that point. The actuation mechanism of PZTs is partially schematized in Fig 1(a). Let E_3 represent the applied electric field along direction *3*. The PZT in the presence of E_3 produces extensional actuations d_{31}, d_{32} along the directions *1* and *2*, respectively, and longitudinal actuation d_{33} along *3*. The reaction forces generated from the structure are measured by the PZT in terms of the admittance $\overline{Y_C}$, which is the inverse of the electrical impedance, and consists of the real term known as conductance (G) and the imaginary term known as susceptance (B). Analytically, the admittance is given as:

$$\overline{Y_C} = G + jB \qquad (j = \sqrt{-1}) \tag{1}$$

A plot of G and B as a function of the actuation frequency serves as a diagnosis of the structure. These plots may present peaks and valleys corresponding to the structural modes of vibrations, thus constituting a unique health signature of the structure. Any change in the mechanical properties of the host element causes changes in the electrical impedance of the PZT. Fig 1(b) shows the signature, i.e. the conductance as a function of the actuation frequency, of one PZT used in this study experimentally and numerically predicted. The frequency peak at about 900 kHz represents the resonant mode of vibration of the transducer within the 0-1 MHz range. The inset shows a close-up view within the frequency range 0 – 800 kHz. Minor peaks concerning the experimental signature are visible. The amplitude of these peaks is two orders of magnitude smaller than the main peak at 900 kHz.

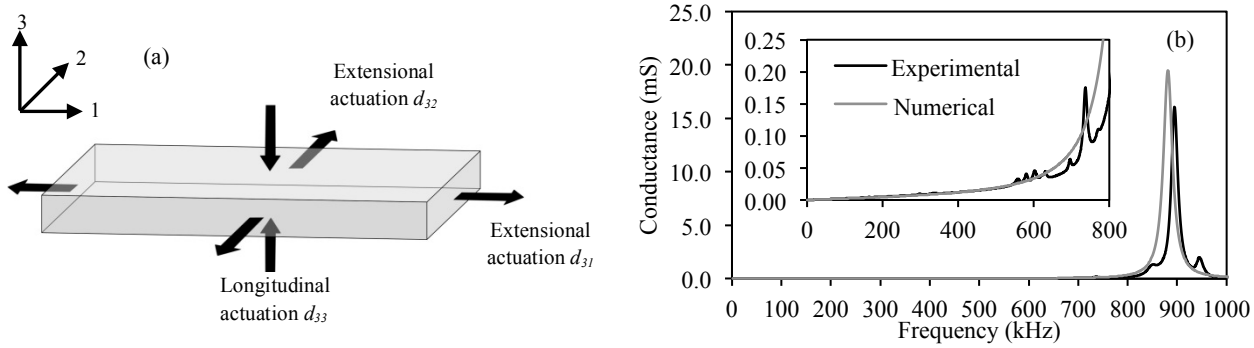

Figure 1. (a) PZT actuation principle. (b) Conductance as a function of the actuation frequency for one PZT used in this study, numerically and experimentally predicted.

3. NUMERICAL SETUP AND RESULTS

In order to predict the interaction between the PZT and the host structure, numerical simulations were developed using the commercial software ANSYS APDL 13.0, performing a couple field analysis (CFA). Many authors applied CFA to simulate the EMI technique [16-17], however, to the best of the authors' knowledge, CFA was never used in the EMI/biomechanical field.

We considered two main models, hereafter indicated as *superstructure* and *superstructure-interface-bone*, respectively. The superstructure aims to reproduce the assembly constituted of a square PSI-5A4E (2x2x0.267 mm) transducer (Piezo Systems, Inc), a permanent prosthetic abutment and a NobelReplace Tapered Groovy (Φ 4.3x13 mm) implant by Nobel Biocare, used experimentally. On the other hand, the superstructure-interface-bone aims to represents the PZT-abutment-implant assembly entrenched into a bone sample (15x15 mm cross section and 20 mm deep). Similarly to [18], we assumed the existence of a 1.5 mm interfacial tissue around the implant as the volume where bone remodeling occurs. The two mentioned models, built and meshed using AUTOCAD and ANSYS, are presented in Fig. 2(a) and (b), respectively. The mesh associated with the superstructure consisted of 3580 nodes and 1784 elements whereas the mesh associated with the superstructure-interface-bone model consisted of 37624 nodes and 25686 elements. Table 1 summarizes the mechanical properties of every component. The bone and the tissue were considered homogeneous and isotropic.

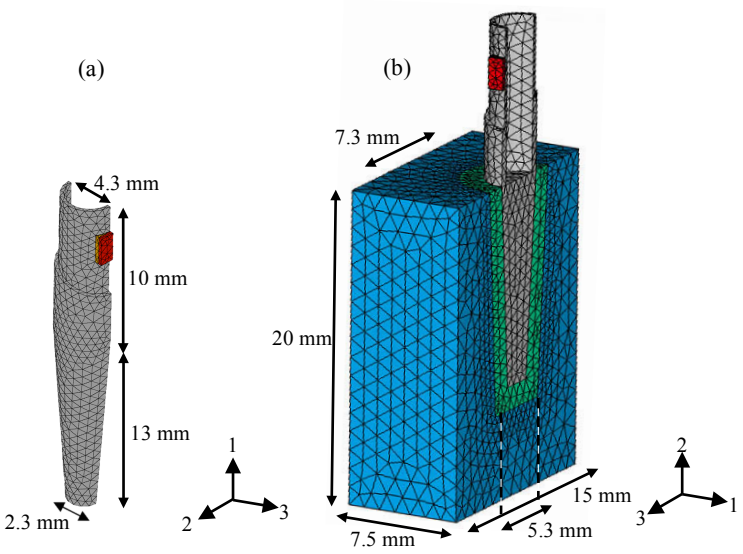

Figure 2. (a) Superstructure. (b) Superstructure-interface-bone.

	PSI-5A4E		Trabecular Bone	Interfacial tissue	Titanium	Epoxy
Density	7800		1000	1000	4506	1000
Poisson ratio	-		0.3	0.3	0.321	0.4
Young's modulus	-		0.25	0.025-0.25	115.7	5.1
Damping ratio	0.0125		0.01	0.01	0.006	-
Rayleigh damping	-		-	-	-	6E-09
Stiffness Matrix [c^E]	C_{11}= C_{22}	152	-	-	-	-
	C_{12}	102				
	C_{13}= C_{23}	100				
	C_{33}	127				
	C_{44}= C_{55}	21				
	C_{66}	25				
Piezoelectric stress matrix [e]	e_{31}= e_{32}	-5.5	-	-	-	-
	e_{33}	16.4				
	e_{24}= e_{15}	12.4				
Electric permittivity matrix [ε^s]	ε_{11}= ε_{22}	950	-	-	-	-
	ε_{33}	890				
Dielectric loss factor	0.02		-	-	-	-

Table 1. Properties of the components of the superstructure-interface-bone system.

To simulate the osseointegration, we assumed the free superstructure as the extreme case of lack of stability (namely 0%), then we analyzed the superstructure-interface-bone by varying the Young's modulus of the interfacial tissue from 25 MPa (namely 10%) to 250 MPa (namely 100% fully osseointegrated), with increments of 10%. The 10-node tetrahedral coupled-field Solid-98 element and the 10-node tetrahedral structural Solid-187 were used for PZT and the host structure, respectively. Owing to the geometric symmetry both of the superstructure and the superstructure-interface-bone, only half system was built. Harmonic analysis was performed in the range 500-1000 kHz, at 0.5 kHz intervals. The selection of this interval represented a good tradeoff between computational efforts and accuracy of results.

Figure 3 shows the conductance as a function of the excitation frequency relative to 0%, i.e. the free superstructure, 10% and 100% degree of osseointegration, i.e. the bonded superstructure-interface-bone. The boundary conditions of the superstructure-interface-bone simulated a portion of jawbone free along the 2-3 plane and fixed along the 1-2 and 1-3 planes. All the signatures in Fig. 3 show one main peak associated with the resonant peak of the PZT and it is about one-fifth in amplitude (Fig. 1(b)). With respect to the conductance signature of the free transducer, Fig. 3 shows new peaks related to the modes of vibration of the host structure. Overall, Fig. 3 does not show any dramatic change associated with the level of osseointegration, but it should be noted that the volume of the interface is about 7% of the volume of the system being analyzed. As often done in the EMI-based structural health monitoring, a close-up view of some structural peak is considered. In particular, the insert shows the conductance as a function of frequencies at range 830-930 kHz associated with two structural peaks, at 868 kHz and 910.5 kHz, respectively. A decrease in amplitude and a slow shift towards higher frequencies is observable.

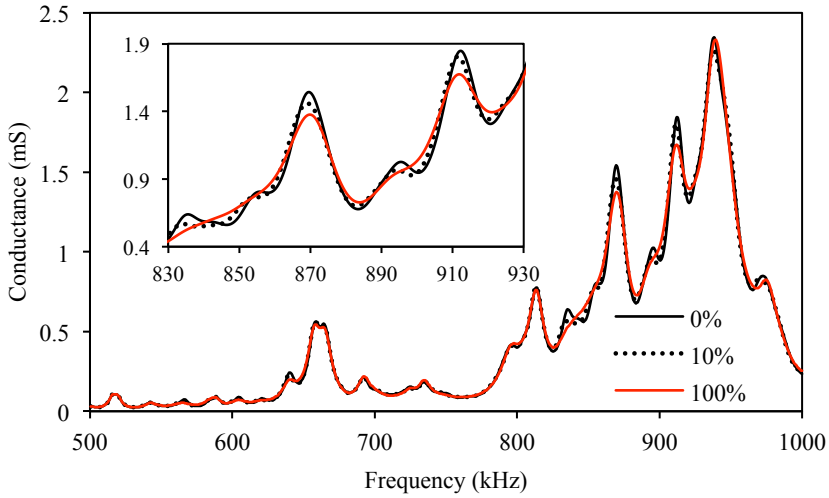

Figure 3. Numerical variation of the interfacial stiffness. Conductance as a function of the actuation frequency obtained for the 0%, 10%, 100% of the bone Young's modulus.

To quantify how conductance peaks are influenced by the stiffness of the interfacial tissue, the main peak at about 950 kHz and the intermediate peak at about 868 kHz peaks are analyzed. For both peaks, the values of the peak amplitude and peak frequency as a function of the Young's modulus are presented in Figs. 4. The plots show that the amplitude has an opposite trend for the two peaks with the interface stiffness. However at both peaks the 0% signature presents the main amplitude. On the other hand, at both frequency peaks the frequency increases with the interface stiffness. Overall, the peaks behavior in terms of frequency is more consistent than in terms of amplitude during modeling of osseointegration.

To better quantify the general effect of the interfacial stiffness variation on the response of the PZT's conductance we calculated the root mean square (RMS) and the root mean square deviation (RMSD) of the conductance signatures.

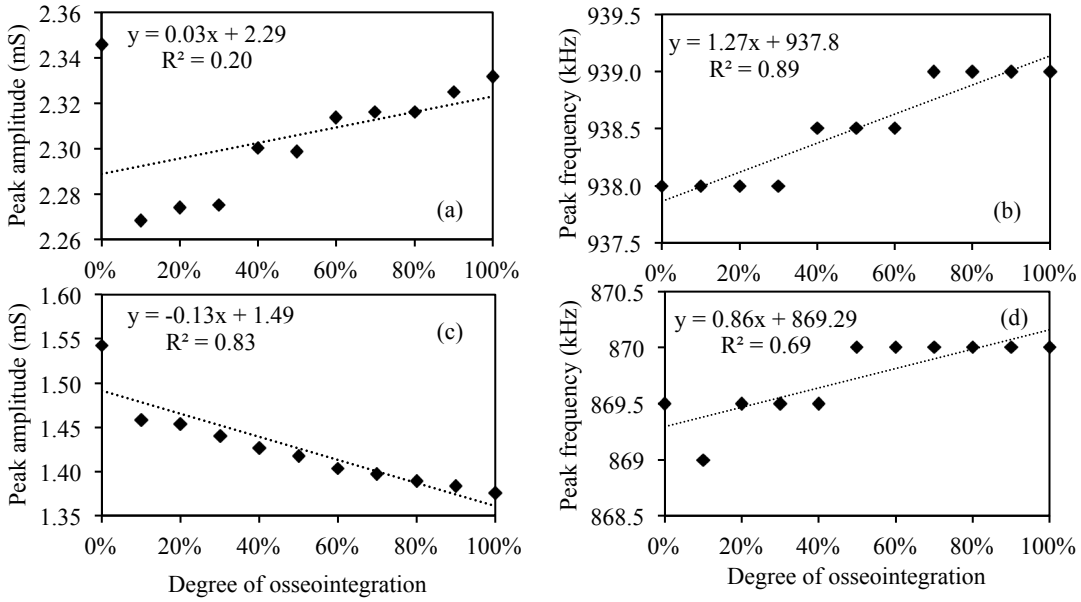

Figure 4. (a) Numerical variation of the interfacial stiffness. (a) Amplitude and (b) frequency of the main peak, (a) Amplitude and (b) frequency of the intermediate peak as a function of the degree of osseointegration.

The RMSD and the RMS of the conductance as a function of the degree of osseointegration are presented in Fig. 5(a) and 5(b), respectively. They were obtained by assuming as baseline the simulation where the interfacial tissue has 10% of the bone Young's modulus. The values presented in Fig. 5(a) are normalized to the baseline value. Both statistical parameters show a monotonic trend, which can be exploited to estimate the degree of osseointegration. Overall, the relative variation between the full osseointegration and the baseline is in the order of -0.4% for the RMS and 4% for the RMSD.

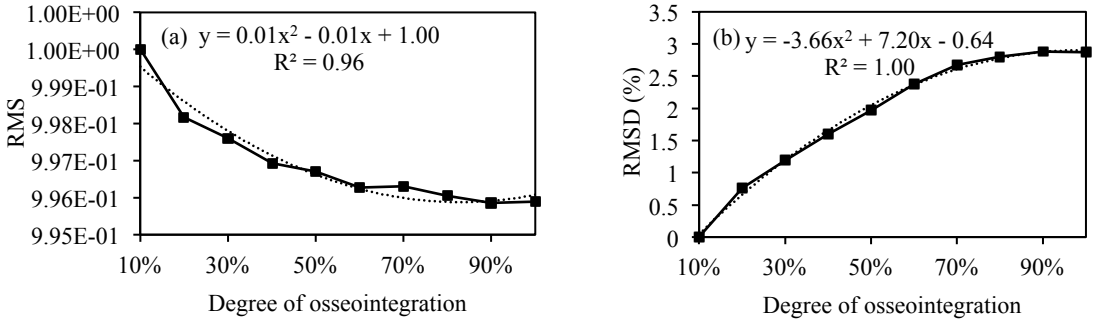

Figure 5. Numerical variation of the interfacial stiffness. (a) RMS and (b) RMSD as a function of the degree of osseointegration.

4. IMPEDANCE MEASUREMENT SYSTEM

In the present study, similarly to [19], the measurement of the electrical impedance of the PZT was taken coupling a low-cost electrical circuit to a NI data acquisition (DAQ) system driven by LabVIEW software. The unknown impedance of the transducer $Z_{unknown}[k]$ is calculated as:

$$Z_{unknown}[k] = \frac{H[k]Z_{in}[k]R_S}{Z_{in}[k] - H[k](R_S + Z_{in}[k])} \tag{2}$$

where R_S is the resistor that controls the voltage across the unknown impedance inside the circuit, $Z_{in}[k]$ is the internal impedance of the DAQ system consisting of a resistance R_P and a capacitance C_P which can be calculated as:

$$Z_{in}[k] = \left(\frac{1}{R_P} + j2\pi k f_{res} C_P \right)^{-1} \tag{3}$$

and $H[k]$ is the frequency response function (FRF) calculated by means of the measured input and output signals as:

$$H[k] = \frac{X_1[k] \cdot X_2[k]}{|X_1[k]|^2} \tag{4}$$

where $X_1[k]$ and $X_2[k]$ are the Discrete Fourier Transforms of the input and output signals, respectively. It should be noted that Eq. (2) is obtained theoretically as the inverse of Eq. (4) by making explicit $X_1[k]$ as a chirp signal and $X_2[k]$ as a function $X_1[k]$ of according to the circuit used. For all the experiments a chirp signal ranging from 0.1 to 1000 kHz was used as an input signal, with number of samples N equal to 200 kS and frequency of sampling f_{res} equal to 10 MHz. This resulted in a frequency resolution of 50 Hz. In Figs. 6(a) and 6(b) the impedance measurement systems and the auxiliary circuit are presented, respectively.

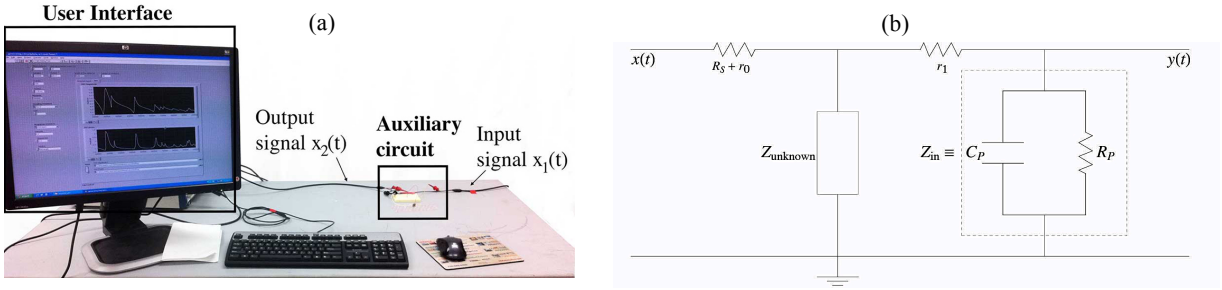

Figure 6. (a) Impedance measurement system built *in house*. (b) Scheme of the circuit used in this study.

5. EXPERIMETAL SETUP

To monitor experimentally the mechanical interlock between an implant and the surrounding bone by means of EMI technique, an *in vitro* bovine bone sample was used. An aesthetic abutment NobRpl 3 mm was screwed to a 13 mm long and 4.3 mm diameter titanium NobelReplace Tapered Groovy implant. Square piezoceramic PSI-5A4E transducer (2×2×0.267 mm) was glued to the abutment by means of epoxy resin. A 5.5 mm diameter, 14 mm deep hole was drilled into the sample. To secure the superstructure to the bone, the commercial root canal sealer Pulp Canal Sealer (PCS) EWT (SybronEndo, Glendora, USA) was used. We assumed that PCS is able to simulate in vitro the process of anchorage of the implant to the bone tissue. The sealer was obtained by mixing the powder with a drop of liquid and was then inserted inside the cavities. Immediately after the insertion of the sealer, the superstructure was carefully inserted in the liquid-filled hole. Figure 7(a) shows the experimental set-up. While curing, the electromechanical properties of the PZT were measured every 15 minutes for 12 hours.

In order to proof the repeatability of the EMI method, we monitored for 11 hours the curing time of the commercial joint compound located inside ten holes created in a specimen made of composite wood, by means of a PZT glued to the surface of a commercial sheet metal screw (12 mm length and 5 mm diameter) made of Zinc. The experimental set-up is presented in Fig. 7(b). To remove the PZT-screw assembly, namely also superstructure, a screwdriver was used. Afterwards, the screw was cleaned.

For all the experiments we assumed the baseline dataset the measurement taken immediately after the insertion of the superstructure (0 h). As such, the baseline can be associated with the case of lack of osseointegration.

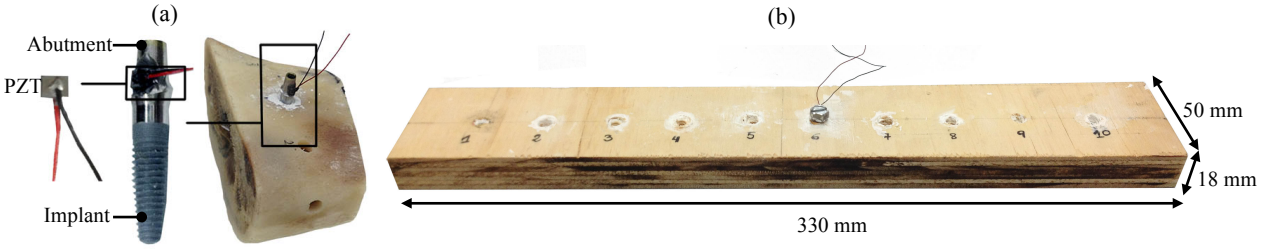

Figure 7. Experimental set-up. (a) Implant/bone test. (b) Screw/wood test.

6. EXPERIMETAL RESULTS

6.1 Implant/Bone test

Figure 8 shows the conductance as a function of the actuation frequency measured for the free superstructure and for the superstructure inserted in the bone at the time of the insertion (0 h) and after 12 hours from the insertion. The main variation of the signature is registered after the superstructure inclusion. This is somehow expected because once inserted the damping of the host structure increases promptly. Hence, the 0 h signature presents less and smaller peaks in terms of amplitude if compared with the free superstructure signature. As long as PCS cures, any dramatic changes are visible. To better quantify the conductance characteristics with the curing time, we focused on the main peak behavior.

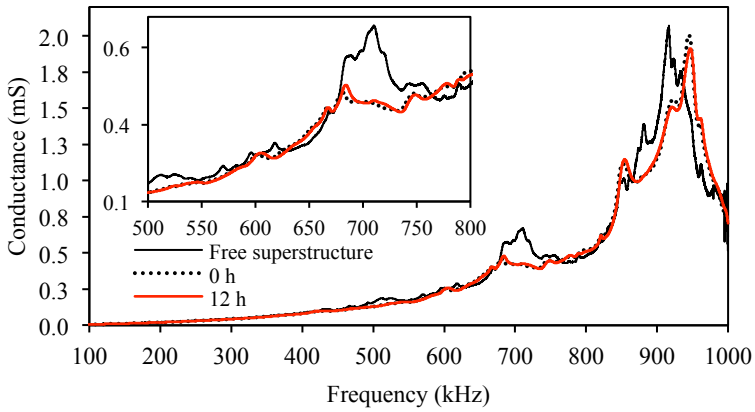

Figure 8. Implant/bone test. Conductance as a function of the actuation frequency obtained for the free superstructure and at the time of the insertion (0h) and after 12 h of inserting.

Figures 9(a) and 9(b) present the amplitude and the frequency as a function of the healing process, respectively. By comparing Fig. 9(a) with the main numerical peak in Fig. 4(a), it is evident that the trend is opposite although the order of magnitude is the same. The plot suggests that the sealer consolidates within the first three hours and then converges asymptotically after seven hours. Contrarily, in both the numerical and experimental responses associated with the frequency peak (Fig. 4(b) and 9(b)), we observe an increase of the frequency of about 1500 Hz and the peak in both cases is located around 940 kHz.

The RMS and RMSD of the conductance signature at the range 5-1000 kHz as a function of the healing time are shown in Figs. 9(c) and 9 (d), respectively. Compared with the corresponding numerical variations of -0.4% (RMS) and 4% (RMSD), we found a good agreement experimentally with -0.7% and 3%.

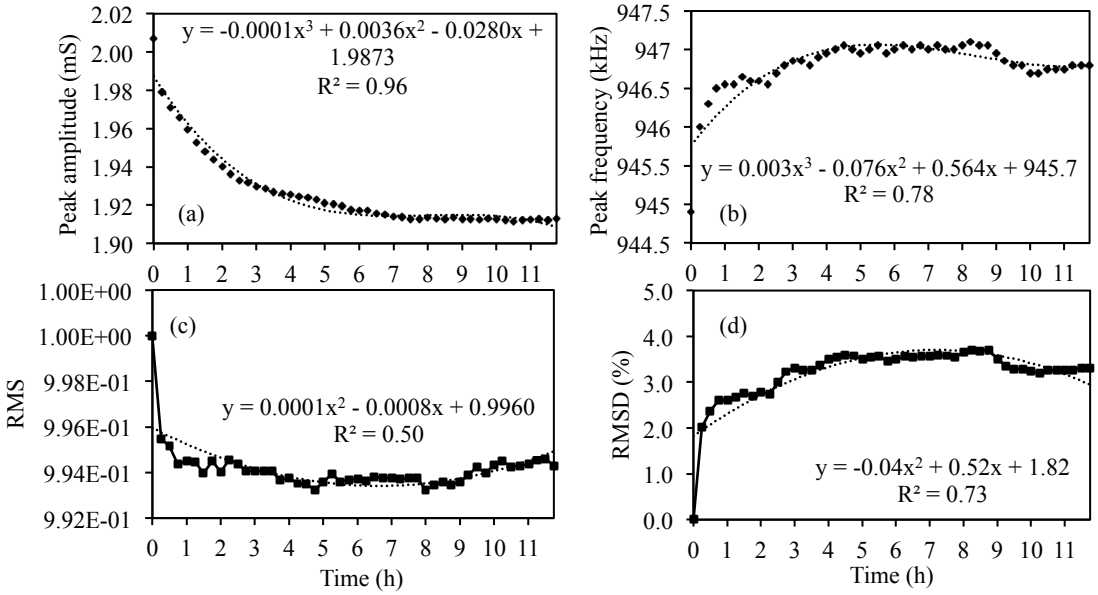

Figure 9. (a) Implant/bone test. (a) Amplitude and (b) frequency of the main peak as a function of the monitoring time of the sealer. (c) RMS and (b) RMSD as a function of the monitoring time of the sealer.

6.2 Screw/Wood test

Figure 10 shows the conductance as a function of the actuation frequency measured for the free superstructure and for the superstructure inserted in the wood at the time of the insertion (0 h) and after 12 hours from the insertion. As for the Implant/Bone test, after the insertion of the screw into the fresh joint compound, the signature changed promptly, as shown in the conductance signature at 0 h. During the healing of the joint compound, the signature gradually damped down and no evident peaks are visible. It can be argued that the PZT dimensions (2x2x0.267 mm) are too small to excite the natural mode of vibrations of the 11h-host structure, which is composed by the assembly of screw and beam.

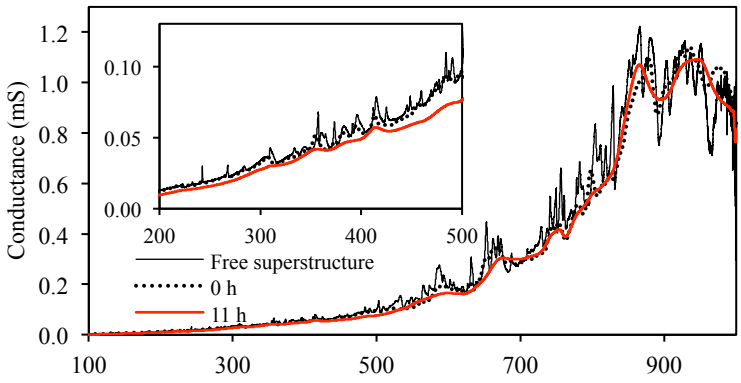

Figure 10. Screw/wood test. Conductance as a function of the actuation frequency obtained for the free superstructure and at the time of the insertion (0h) and after 12 h of inserting.

From 0 h to 11 h the main peak is registered around 940 kHz. Its amplitude and frequency are therefore analyzed, as shown in Figs. 11(a) and (b) respectively. Asymptotic decrease in the amplitude and linear increase in the frequency occur with the curing. The shift of higher frequency is a result in agreement with the numerical and the Implant/Bone test.

RMS and RMSD were calculated in the range from 5 kHz and 900 kHz and are shown in Figs. 11(c) and 11(d) as a function of the curing time for eight different monitoring tests. The RMS variations range from -2.3% (Hole 8) to 1.3% (Hole 6) whereas the RMSD variations range from 4% (Hole 7) to 9% (Hole 4). The trend is the same even though there is a shift between the experiments that may be relative to small variations of the experimental set-up.

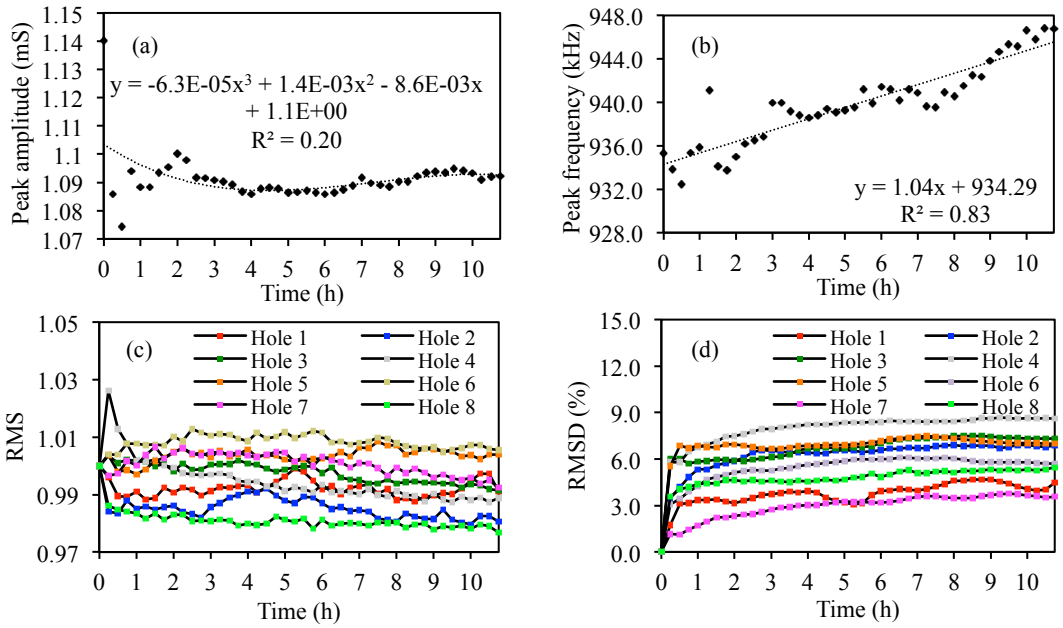

Figure 11. (a) Screw/wood test. (a) Amplitude and (b) frequency of the main peak as a function of the monitoring time of the joint compound. (c) RMS and (b) RMSD as a function of the monitoring time of the joint compound.

7. CONCLUSIONS

In this paper we propose the advancements of the study conducted in the past few years on the electromechanical impedance (EMI) method to monitor the stability of dental implants after surgical placement. The clinical approach hypothesizes that a piezoelectric transducer (PZT) bonded to the abutment screwed to the implant to be monitored can assess the degree of healing of the tissue in the weeks subsequent to the surgery. In fact, when subjected to an electric field, the transducer induces structural excitations which affect the transducer's electrical admittance. As the structural vibrations depend on the mechanical interlock between the implant and the surrounding bone, the measurement of the PZT's admittance can be exploited to diagnose the implant therapy.

We conducted a numerical analysis and a series of experiments aimed at validating the above research hypotheses. A 3D finite element model of a PZT bonded to the abutment of a dental implant placed in the host bone site was created in ANSYS to simulate the progress of the tissue healing dynamics that occurs after an implant is surgical inserted. The healing was modeled by changing the Young's modulus of a 1.5 mm bone-implant interface. Experimentally, dental implants with a specific geometry were entrenched in two in vitro bone samples. The mechanical interlock between the implant and the bone was induced by inserting a root canal sealer, whose curing was monitored by bonding a PZT to the side of an abutment secured to the implant and measuring the electrical admittance of the transducer. The results demonstrated that as the curing progresses, the characteristics of the electrical conductance change. The experimental results were also interpreted by comparing them to the numerical ones. We found that most of the experimental and numerical results are in good agreement each other.

ACKNOWLEDGMENTS

The first and the third authors conducted this research as a visiting scholar at the University of Pittsburgh's Laboratory for Nondestructive Evaluation and Structural Health Monitoring studies thanks to the scholarship "Borse di studio finalizzate alla ricerca e Assegni finanziati da Programmi Comunitari" provided by the University of Palermo, Italy. Most of the equipment used in this study was purchased through a U.S. National Science Foundation grant (CMMI 1029457).

REFERENCES

[1] Bahat, O., "Brånemark system implants in the posterior maxilla: a clinical study of 660 implants followed fro 5 to 12 years," Int. J. Oral Maxillofac. Implants 15, 646-653 (2000).

[2] Brånemark, P. I., Breine, U., Adell, R., Hansson, B. O., Lindström, J. and Ohlsson, Å., "Intra-osseous anchorage of dental prostheses: I. experimental studies," Scandinavian Journal of Plastic and Reconstructive Surgery and Hand Surgery 3(2), 81-100 (1969).

[3] Javed, F. and Romanos, G. E., "The role of primary stability for successful immediate loading of dental implants. A literature review," Journal of dentistry 38(8), 612-620 (2010).

[4] Mavrogenis, A. F., Dimitriou, R., Parvizi, J. and Babis, G. C., "Biology of implant osseointegration," J. Musculoskelet Neuronal Interact 9(2), 61-71 (2009).

[5] Blanes, R. J., Bernard, J. P., Blanes, Z. M. and Belser, U. C., "A 10-year prospective study of ITI dental implants placed in the posterior region. I: Clinical and radiographic results," Clinical oral implants research 18(6), 699-706 (2007).

[6] Wang, Z., Zhao, Z., Xue, J., Song. J., Deng, F. and Yang, P., "Pullout strength of miniscrews placed in anterior mandibles of adult and adolescent dogs: a microcomputed tomographic analysis," American Journal of Orthodontics and Dentofacial Orthopedics 137(1), 100-107 (2010).

[7] Schulte, W., d'Hoedt, B., Lukas, D., Muhlbradt, L., Scholz, F., Bretschi, J., Frey, D., Gudat, H., Konig, M. and Markl, M., "Periotest--a new measurement process for periodontal function," Zahnarztliche Mitteilungen, 73(11) 1229-30 (1983).

[8] Meredith, N., "Assessment of implant stability as a prognostic determinant," The International journal of prosthodontics, 11(5) 491-501 (1997).

[9] Hayashi, M., Kobayashi, C., Ogata, H., Yamaoka, M. and Ogiso, B., "A no-contact vibration device for measuring implant stability," Clinical Oral Implants Research, 21(9) 931-936 (2010).

[10] Aparicio, C., Lang, N.P. and Rangert, B., "Validity and clinical significance of biomechanical testing of implant/bone interface," Clinical Oral Implants Research 17(S2), 2-7 (2006).

[11] Boemio, G., Rizzo, P. and De Nardo, L., “Assessment of dental implant stability by means of the electromechanical impedance method,” Smart Materials and Structures 20(4), 045008 (2011).
[12] Tabrizi, A., Rizzo, P. and Ochs, M. W., “Electromechanical impedance method to assess dental implant stability,” Smart Materials and Structures 21(11), 115022 (2012).
[13] Park, G., Sohn, H., Farrar, C.R. and Inman, D.J., “Overview of piezoelectric impedance-based health monitoring and path forward,” Shock and Vibration Digest 35(6), 451-464 (2003).
[14] Soh, C.K., Yang, Y. and Bhalla, S., [Smart Materials in Structural Health Monitoring, Control and Biomechanics], Springer, (2012).
[15] Soh C.K,. Yang Y. and Bhalla S., [Smart Materials in Structural Health Monitoring, Control and Biomechanics], Springer, 569-581 (2012).
[16] Yang, Y., Lim, Y. Y. and Soh, C. K., “Practical issues related to the application of the electromechanical impedance technique in the structural health monitoring of civil structures: II. Numerical verification,” Smart Materials and Structures 17, 1-12 (2008).
[17] Liu W. and Giurgiutiu V., "Finite element simulation of piezoelectric wafer active sensors for structural health monitoring with coupled-filed elements," Proc. SPIE, 65293R-65293R (2007).
[18] Wang, S., Liu, G. R., Hoang, K. C. and Guo, Y., “Identifiable range of osseointegration of dental implants through resonance frequency analysis,” Medical engineering & physics 32(10), 1094-1106 (2010).
[19] Baptista, F. G. and Filho, J. V., “A new impedance measurement system for PZT-based structural health monitoring,” IEEE Transactions on Instrumentation and Measurement 58(10), 3602-3608 (2009).
[20] La Malfa Ribolla, E., Rizzo, P. and Gulizzi, V., “On the use of the electromechanical impedance method for the assessment of dental implant stability. Part I: Modeling,” (2013) *in review*.
[21] La Malfa Ribolla, E., Rizzo, P. and Gulizzi, V., “On the use of the electromechanical impedance method for the assessment of dental implant stability. Part II: Experimental study,” (2013) *in review*.